

## Oblique Stagnation-Point Flow Past a Shrinking Surface in a Cu-Al<sub>2</sub>O<sub>3</sub>/H<sub>2</sub>O Hybrid Nanofluid

(Aliran Titik Genangan Serong Nanobendalir Hibrid Cu-Al<sub>2</sub>O<sub>3</sub>/H<sub>2</sub>O terhadap Permukaan Mengecut)

RUSYA IRYANTI YAHAYA, NORIHAN MD ARIFIN\*, ROSLINDA MOHD. NAZAR & IOAN POP

### ABSTRACT

*To fill the existing literature gap, the numerical solutions for the oblique stagnation-point flow of Cu-Al<sub>2</sub>O<sub>3</sub>/H<sub>2</sub>O hybrid nanofluid past a shrinking surface are computed and analyzed. The computation, using similarity transformation and bvp4c solver, results in dual solutions. Stability analysis then shows that the first solution is stable with positive smallest eigenvalues. Besides that, the addition of Al<sub>2</sub>O<sub>3</sub> nanoparticles into the Cu-H<sub>2</sub>O nanofluid is found to reduce the skin friction coefficient by 37.753% while enhances the local Nusselt number by 4.798%. The increase in the shrinking parameter reduces the velocity profile but increases the temperature profile of the hybrid nanofluid. Meanwhile, the increase in the free parameter related to the shear flow reduces the oblique flow skin friction.*

*Keywords: Dual solutions; hybrid nanofluid; oblique stagnation-point; shrinking surface; stability analysis*

### ABSTRAK

*Bagi memenuhi jurang kepustakaan sedia ada, penyelesaian numerik bagi aliran titik genangan serong nanobendalir hibrid Cu-Al<sub>2</sub>O<sub>3</sub>/H<sub>2</sub>O terhadap permukaan mengecut telah dihitung dan dianalisis. Pengiraan menggunakan penjelmaan keserupaan dan fungsi bvp4c telah menghasilkan penyelesaian dual. Hasil analisis kestabilan menunjukkan bahawa penyelesaian pertama adalah stabil dengan nilai eigen terkecil positif. Secara puratanya, penambahan nanozarah Al<sub>2</sub>O<sub>3</sub> ke dalam nanobendalir Cu-H<sub>2</sub>O telah mengurangkan pekali geseran kulit sebanyak 37.753% dan meningkatkan nombor Nusselt tempatan sebanyak 4.798%. Peningkatan parameter mengecut pula dilihat mengurangkan profil halaju nanobendalir hibrid tetapi menyebabkan profil suhunya meningkat. Sementara itu, peningkatan nilai parameter bebas berkaitan aliran sesar telah mengurangkan geseran kulit aliran serong.*

*Kata kunci: Aliran titik genangan serong; analisis kestabilan; nanobendalir hibrid; penyelesaian dual; permukaan mengecut*

### INTRODUCTION

Hybrid nanofluid, an extension to nanofluid, consists of two or more different nanoparticles (e.g. Cu-Al<sub>2</sub>O<sub>3</sub>, TiO<sub>2</sub>-Cu & Ag-CuO) dispersed in a conventional base fluid (e.g. polymer solutions, water (H<sub>2</sub>O), oil and ethylene glycol (EG)). The hybrid nanofluid is predicted to be more superior than regular heat transfer fluids and nanofluids, thus prompting research on the thermophysical properties, rheological behavior, and applications of this new generation of nanofluid. Generally, hybrid nanofluids are prepared through single-step method (i.e. suitable for small scale production) or two-step method (i.e. suitable for mass production), as described by Sidik et al. (2016). One of the pioneering studies on hybrid nanofluid is

probably by Turcu et al. (2006) with Fe<sub>3</sub>O<sub>4</sub> added into multi wall carbon nanotubes (MWCNTs). Suresh et al. (2012) then discussed the preparation of water-based hybrid Al<sub>2</sub>O<sub>3</sub>-Cu nanofluid and did experimental investigations on the heat transfer and friction characteristics of the fluid. The Nusselt number, which corresponds to the heat transfer performance, for the water-based hybrid nanofluid is found to be higher than pure water and Al<sub>2</sub>O<sub>3</sub>-H<sub>2</sub>O nanofluid. Also, the friction factor of the hybrid nanofluid is slightly higher than the nanofluid, due to the higher viscosity of the hybrid nanofluid. The applications of hybrid nanofluid include electronic cooling, domestic refrigerator, car radiators, and nuclear plant (Sidik et al. 2016). The magnetic field effects on the flow of water-based

$\text{Al}_2\text{O}_3$ -Cu hybrid nanofluid past a permeable sheet with stretching velocity is studied by Devi and Devi (2016). In this study, new thermophysical properties, which are in good agreement with the experimental results by Suresh et al. (2012), are developed to study the boundary layer equations for the hybrid nanofluid. From this study, it was concluded that the presence of the magnetic field increases the heat transfer rate and makes the flow consistent. Hayat et al. (2018) then analyzed the thermal radiation, thermal slip, and velocity slip effects on the rotating Ag-CuO/water hybrid nanofluid. In recent years, Jamaludin et al. (2020), Kadhim et al. (2020), Khashi'ie et al. (2020), and Waini et al. (2020) had conducted several other studies on hybrid nanofluid.

The classical two-dimensional stagnation-point flow, first studied by Hiemenz (1911), describes the flow of fluid striking on a solid surface orthogonally. The solid surface can be stationary or moving with stretching or shrinking velocity. This type of flow is common in the cooling process of nuclear reactors and electronic devices, extrusion of polymer and plastic sheets, and wire drawing (Sadiq 2019). However, in some cases, the flow impinges the solid surface obliquely and produces an oblique stagnation-point flow. According to Wang (1985), this flow may occur due to the contouring of the solid surface or physical constraints on the nozzle. Besides that, the reattachment of separated viscous flow to a surface may also bring about an oblique stagnation-point flow (Reza & Gupta 2010). The oblique or non-orthogonal stagnation-point flow is made up of the orthogonal stagnation-point flow (i.e. normal to the solid surface) and shear flow (i.e. parallel to the solid surface). The pioneering study, made by Stuart (1959), found that the part of the shear that is proportional to vorticity is larger in the external stream than at the wall. Later, Dorrepaal (1986) and Tamada (1979) revisited the problem with more detailed discussions on the structure of the flow field. Meanwhile, Wang (1985) studied the unsteady flow. In 2006, Drazin and Riley introduced a free parameter for the shear flow component. This free parameter changes the shear flow by altering the magnitude of the pressure gradient parallel to the solid surface. Then, Tooke and Blyth (2008) found that large adverse pressure gradient causes reverse flow near the solid surface. Labropulu and Li (2008) then did a study on the slip effects. The heat transfer in oblique stagnation-point flow was studied by Li et al. (2009) and Lok et al. (2009) over an infinite plane and a vertical stretching sheet, respectively. Meanwhile, Grosan et al. (2009) analyzed the magnetic field effects on the flow. The increase in the magnetic field was observed to reduce the displacement of the stagnation-point from the origin.

Lok et al. (2015) then extended this study for stretching/shrinking surface.

Through our reviews, the oblique stagnation-point flow of nanofluid had been discussed by Ghaffari et al. (2017), Mahmood et al. (2017), Nadeem et al. (2019), and Rahman et al. (2016). However, the study for this kind of flow on hybrid nanofluid had not been done by any researchers yet. We aim to fill this literature gap in the current study. The findings in the present study are useful in predicting the behavior of hybrid nanofluid in such flow and relevant parameters affecting the heat transfer performance of this fluid; this might be important for potential applications of hybrid nanofluid in the future.

Inspired by the previous studies, the oblique stagnation-point flow of hybrid nanofluid will be considered in the current study. The flow of Cu- $\text{Al}_2\text{O}_3$ /H<sub>2</sub>O hybrid nanofluid over a shrinking surface will be analyzed and discussed. Numerical solutions to the problem will be computed using MATLAB's built-in solver, *bvp4c*.

#### PROBLEM FORMULATION

Let us consider the two-dimensional, steady, laminar stagnation-point flow of hybrid nanofluid, Cu- $\text{Al}_2\text{O}_3$ /H<sub>2</sub>O impinges obliquely on a shrinking surface. The axes,  $x$  and  $y$  are dimensional Cartesian coordinates with the  $x$ -axis lined along the surface and  $y$ -axis perpendicular to it, as illustrated in Figure 1. The shrinking surface velocity is assumed to be  $u_w(x) = cx$ , where  $c < 0$ . Meanwhile, the external flow is given as the following stream function,  $\psi$  (Drazin & Riley 2006; Tooke & Blyth 2008):

$$\psi = a x y + \frac{b}{2} y^2, \quad (1)$$

with  $a$  and  $b (> 0)$  as the irrotational straining flow strength and the rotational shear flow vorticity, respectively. From (1),  $y = -2(a/b)x$  is the dividing streamline ( $\psi = 0$ ) that intersects the surface  $y = 0$ . From the usual definition of stream function,  $\partial \psi / \partial y = u$  and  $-\partial \psi / \partial x = v$  the external flow velocities are given by:

$$u_e(x, y) = a x + b y \text{ and } v_e(y) = -a y, \quad (2)$$

The basic equations of this problem are Devi and Devi (2017) and Lok et al. (2015):

$$\frac{\partial u}{\partial x} + \frac{\partial v}{\partial y} = 0, \quad (3)$$

$$u \frac{\partial u}{\partial x} + v \frac{\partial u}{\partial y} = -\frac{1}{\rho_{hnf}} \frac{\partial p}{\partial x} + \frac{\mu_{hnf}}{\rho_{hnf}} \nabla^2 u, \quad (4)$$

$$u \frac{\partial v}{\partial x} + v \frac{\partial v}{\partial y} = - \frac{1}{\rho_{hnf}} \frac{\partial p}{\partial y} + \frac{\mu_{hnf}}{\rho_{hnf}} \nabla^2 v, \quad (5)$$

$$u \frac{\partial T}{\partial x} + v \frac{\partial T}{\partial y} = \frac{k_{hnf}}{(\rho C_p)_{hnf}} \nabla^2 T, \quad (6)$$

with the boundary conditions:

$$v = 0, \quad u = u_w(x), \quad T = T_w \quad \text{at} \quad y = 0, \quad (7)$$

$$u \rightarrow u_e(x, y), \quad v \rightarrow v_e(y), \quad T \rightarrow T_\infty \quad \text{as} \quad y \rightarrow \infty,$$

where the horizontal and vertical velocity components are given by  $u$  and  $v$ , respectively,  $p$  is the pressure,  $T$  is the hybrid nanofluid temperature and  $\nabla^2$

$= \partial^2/\partial x^2 + \partial^2/\partial y^2$  is the Laplacian. Here,  $\mu_{hnf}$ ,  $k_{hnf}$ , and  $\rho_{hnf}$  are the dynamic viscosity, thermal conductivity and density of the hybrid nanofluid, respectively. Meanwhile,  $(C_p)_{hnf}$  is the specific heat of the hybrid nanofluid. The definition of these parameters is given in Devi and Devi (2017).

Initially, 0.1 vol. of  $Al_2O_3$  (aluminum oxide) nanoparticles (i.e.  $\phi_{s1} = 0.1$ ), which is fixed throughout the problem hereafter, is dispersed into the base fluid,  $H_2O$  to form  $Al_2O_3-H_2O$ . Then, Cu (copper) is added with various solid volume fractions,  $\phi_{s2}$  to produce a hybrid nanofluid named  $Cu-Al_2O_3/H_2O$ . The final form of the effective thermophysical properties of the base fluid and nanoparticles are shown in Table 1.

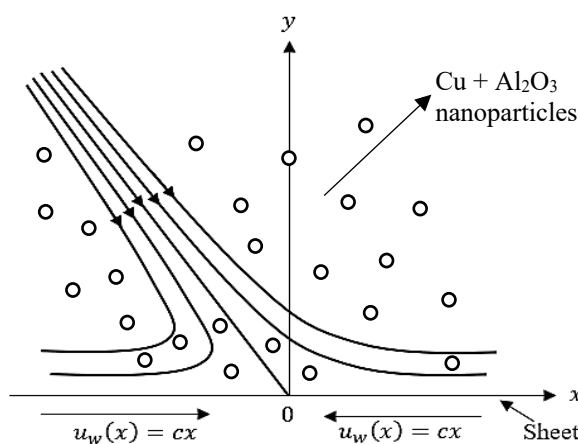


FIGURE 1. Geometry of the problem

TABLE 1. Thermo-physical properties

Physical properties	Water	$Al_2O_3$	Cu
$\rho$ ( $kg/m^3$ )	997.0	3970	8933
$C_p$ ( $J/kgK$ )	4180	765	385
$k$ ( $W/mK$ )	0.6071	40	400

Source: Devi and Devi 2017

Next, the pressure,  $p$  in equations (4) and (5) is eliminated to obtain:

$$\frac{\partial \psi}{\partial x} \frac{\partial}{\partial y} (\nabla^2 \psi) - \frac{\partial \psi}{\partial y} \frac{\partial}{\partial x} (\nabla^2 \psi) = \frac{\mu_{hnf}}{\rho_{hnf}} \nabla^2 (\nabla^2 \psi), \quad (8)$$

$$\frac{\partial \psi}{\partial y} \frac{\partial T}{\partial x} - \frac{\partial \psi}{\partial x} \frac{\partial T}{\partial y} = \frac{k_{hnf}}{(\rho C_p)_{hnf}} \nabla^2 T, \quad (9)$$

subject to the boundary conditions:

$$\psi = 0, \quad \frac{\partial \psi}{\partial y} = cx, \quad T = T_w \quad \text{at} \quad y = 0, \quad (10)$$

$$\psi \rightarrow axy + \frac{1}{2}by^2, \quad T \rightarrow T_\infty \quad \text{as} \quad y \rightarrow \infty.$$

We look for similarity solutions of (8) and (9) in the more general form. Based on Drazin and Riley (2006), Lok

et al. (2015), and Tooke and Blyth (2008):

$$\psi = (a v_f)^{1/2} x f(\eta) + \frac{b v_f}{a} \int_0^\eta g(s) ds, \tag{11}$$

$$\theta(\eta) = \frac{T - T_\infty}{\Delta T}, \quad \eta = y \left( \frac{a}{v_f} \right)^{1/2},$$

with  $\nabla T = T_w - T_\infty$ . Then, the following equations are obtained by substituting (11) into (8) and (9), and equating the terms with  $x$  and those without  $x$ :

$$\frac{\mu_{hnf}/\mu_f}{\rho_{hnf}/\rho_f} f^{(4)} + f f''' - f' f'' = 0, \tag{12}$$

$$\frac{\mu_{hnf}/\mu_f}{\rho_{hnf}/\rho_f} g''' + f g'' - f'' g = 0, \tag{13}$$

$$\frac{1}{Pr} \frac{k_{hnf}/k_f}{(\rho C_p)_{hnf}/(\rho C_p)_f} \theta'' + f \theta' = 0. \tag{14}$$

It requires that  $f(\eta) \sim \eta - \alpha$  and  $g(\eta) \sim \eta - \beta$ , with  $\alpha$  and  $\beta$  as constants, to match with the external flow (1). We integrate (12) and (13) with respect to  $\eta$  and utilize the conditions at  $\eta \rightarrow \infty$  to have:

$$\frac{1}{(1 - \phi_{s1})^{2.5} (1 - \phi_{s2})^{2.5} \left[ (1 - \phi_{s2}) \left[ (1 - \phi_{s1}) + \phi_{s1} \frac{\rho_{s1}}{\rho_f} \right] + \phi_{s2} \frac{\rho_{s2}}{\rho_f} \right]} f''' + f f'' + 1 = 0, \tag{15}$$

$$\frac{1}{(1 - \phi_{s1})^{2.5} (1 - \phi_{s2})^{2.5} \left[ (1 - \phi_{s2}) \left[ (1 - \phi_{s1}) + \phi_{s1} \frac{\rho_{s1}}{\rho_f} \right] + \phi_{s2} \frac{\rho_{s2}}{\rho_f} \right]} g'' + f g' - f' g + \alpha = 0, \tag{16}$$

$$\frac{1}{Pr \left[ (1 - \phi_{s2}) \left[ (1 - \phi_{s1}) + \phi_{s1} \frac{(\rho C_p)_{s1}}{(\rho C_p)_f} \right] + \phi_{s2} \frac{(\rho C_p)_{s2}}{(\rho C_p)_f} \right]} \theta'' + f \theta' = 0. \tag{17}$$

Now, the boundary conditions (10) become:

$$f(\eta) = 0, \quad f'(\eta) = \lambda, \quad g(\eta) = 0, \quad \theta(\eta) = 1 \quad \text{at} \quad \eta = 0,$$

$$f'(\eta) \rightarrow 1, \quad g'(\eta) \rightarrow 1, \quad \theta(\eta) \rightarrow 0 \quad \text{as} \quad \eta \rightarrow \infty. \tag{18}$$

From these equations, " ' " represents differentiation with respect to the similarity variable,  $\eta$  and  $\lambda = c/a$  is the shrinking parameter with  $\lambda < 0$ . The numerical values of  $\alpha$ , tabulated in Table 2, are computed by solving the orthogonal stagnation-point (15) along with the boundary conditions (18). As  $\phi_{s1} = \phi_{s2} = \lambda = 0$ , the value of  $\alpha$  agrees with the ones obtained by Rahman et al. (2016). Meanwhile, the free parameter  $\beta$  is related to the oblique flow (Drazin & Riley 2006; Tooke & Blyth 2008). It should be mentioned that (15) and (17) reduce to (12) and (20) from Mahapatra and Gupta (2002) when  $\phi_{s1} = \phi_{s2} = 0$  and  $\lambda = 1$  (stretching sheet).

The streamlines can be plotted using the following dimensionless stream function:

$$\frac{\psi}{v_f} = \xi f(\eta) + \frac{b}{a} \int_0^\eta g(s) ds, \tag{19}$$

with  $\xi = (a/v_f)^{1/2} x$ . The stagnation point where the dividing streamline  $\frac{\psi}{v_f} = 0$  meets the surface is denoted by  $\xi_0$ . However, the obtained location of  $\xi_0$  will not be exactly on the sheet surface ( $\eta = 0$ ). The reason is that the condition  $f(0) = 0$  from (18) leads to a division by zero. The streamlines are plotted in Figures 2 and 3.

The heat flux,  $q_w$  and the skin friction,  $\tau_w$  are:

$$q_w = -k_{hnf} \left( \frac{\partial T}{\partial y} \right)_{y=0}, \quad \tau_w = \mu_{hnf} \left( \frac{\partial u}{\partial y} \right)_{y=0}. \tag{20}$$

We have, in dimensionless form:

$$Re_x^{-1/2} Nu_x = - \frac{k_{hnf}}{k_f} \theta'(0), \quad Re_x C_f = \frac{\mu_{hnf}}{\mu_f} \left[ \xi f''(0) + \frac{b}{a} g'(0) \right], \tag{21}$$

where  $Nu_x = x q_w / (k_f (T_w - T_\infty))$  is the local Nusselt number,  $C_f = \tau_w / (\rho_f (ax)^2)$  is the skin friction coefficient and  $Re_x = \frac{ax^2}{\nu_f} = \xi^2$  is the local Reynolds number.

TABLE 2. Numerical values of  $\alpha$  for various values of  $\phi_{s1}$ ,  $\phi_{s2}$  and  $\lambda$

$\phi_{s1}$	$\phi_{s2}$	$\lambda$	$\alpha$	
			First solution	Second solution
0	0	0	0.647900	-
0.1	0.005	-1.06	2.122097	9.713256
		-1.04	2.061744	11.735493
		-1.02	2.005328	16.236499

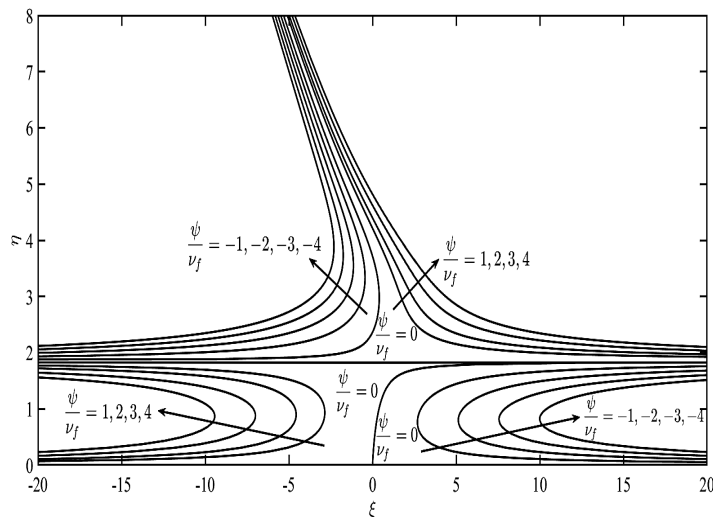


FIGURE 2. Streamlines when  $\lambda = -1.02$ ,  $\alpha = \beta = 2.005328$  and  $\frac{b}{a} = 2$

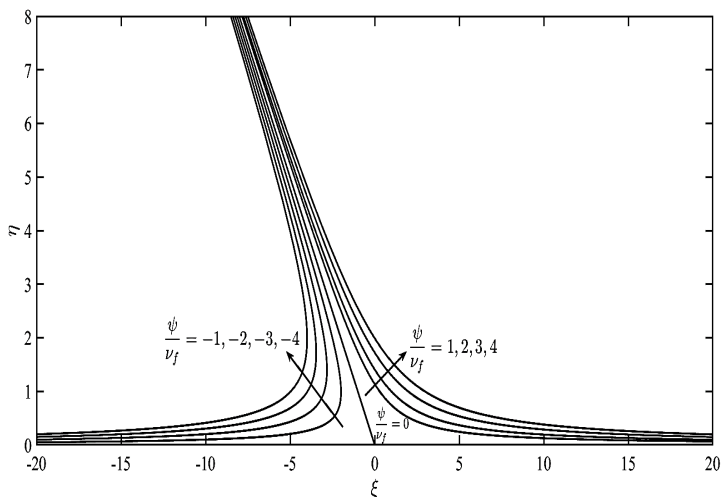


FIGURE 3. Streamlines when  $\lambda = 1.02$ ,  $\alpha = \beta = -0.010530$  and  $\frac{b}{a} = 2$

STABILITY ANALYSIS OF SOLUTIONS

The stability and significance of the solutions can be ascertained through a stability analysis. Following the study by Kamal et al. (2019), Lok et al. (2018), and Naganthran et al. (2017), the analysis is performed by examining the present problem as unsteady or time-dependent:

$$\frac{\partial u}{\partial t} + u \frac{\partial u}{\partial x} + v \frac{\partial u}{\partial y} = -\frac{1}{\rho_{hnf}} \frac{\partial p}{\partial x} + \frac{\mu_{hnf}}{\rho_{hnf}} \nabla^2 u, \quad (22)$$

$$\frac{\partial v}{\partial t} + u \frac{\partial v}{\partial x} + v \frac{\partial v}{\partial y} = -\frac{1}{\rho_{hnf}} \frac{\partial p}{\partial y} + \frac{\mu_{hnf}}{\rho_{hnf}} \nabla^2 v, \quad (23)$$

$$\frac{\partial T}{\partial t} + u \frac{\partial T}{\partial x} + v \frac{\partial T}{\partial y} = \frac{k_{hnf}}{(\rho C_p)_{hnf}} \nabla^2 T, \quad (24)$$

where  $t$  is for time. In the similarity solutions (11),  $\tau$ , which is a dimensionless time variable, is introduced to form:

$$\begin{aligned} \psi &= (a v_f)^{1/2} x f(\eta, \tau) + \frac{b v_f}{a} \int_0^\eta g(s, \tau) ds, \\ \theta(\eta, \tau) &= \frac{T - T_\infty}{\Delta T}, \quad \eta = y \left( \frac{a}{v_f} \right)^{1/2}, \quad \tau = at. \end{aligned} \quad (25)$$

Substituting (25) into equations (22) to (24) results to the following equations:

$$\frac{\mu_{hnf}/\mu_f}{\rho_{hnf}/\rho_f} \frac{\partial^3 f}{\partial \eta^3} + f \frac{\partial^2 f}{\partial \eta^2} - \left( \frac{\partial f}{\partial \eta} \right)^2 - \frac{\partial^2 f}{\partial \eta \partial \tau} + 1 = 0, \quad (26)$$

$$\frac{\mu_{hnf}/\mu_f}{\rho_{hnf}/\rho_f} \frac{\partial^2 g}{\partial \eta^2} - g \frac{\partial f}{\partial \eta} + f \frac{\partial g}{\partial \eta} - \frac{\partial g}{\partial \tau} + \alpha - \beta = 0, \quad (27)$$

$$\frac{1}{Pr} \frac{k_{hnf}/k_f}{(\rho C_p)_{hnf}/(\rho C_p)_f} \frac{\partial^2 \theta}{\partial \eta^2} + f \frac{\partial \theta}{\partial \eta} - \frac{\partial \theta}{\partial \tau} = 0, \quad (28)$$

$$f(0, \tau) = 0, \quad \frac{\partial}{\partial \eta} f(0, \tau) = \lambda, \quad g(0, \tau) = 0, \quad \theta(0, \tau) = 1 \quad (29)$$

$$\frac{\partial}{\partial \eta} f(\eta, \tau) \rightarrow 1, \quad \frac{\partial}{\partial \eta} g(\eta, \tau) \rightarrow 1, \quad \theta(\eta, \tau) \rightarrow 0 \quad \text{as } \eta \rightarrow \infty.$$

Next, the following time-dependent solutions are introduced to examine the stability of the solutions  $f(\eta) = f_0(\eta)$ ,  $g(\eta) = g_0(\eta)$  and  $\theta(\eta) = \theta_0(\eta)$  (Weidman et al. 2006):

$$\begin{aligned} f(\eta, \tau) &= f_0(\eta) + e^{-\varepsilon\tau} F(\eta, \tau), \\ g(\eta, \tau) &= g_0(\eta) + e^{-\varepsilon\tau} G(\eta, \tau), \\ \theta(\eta, \tau) &= \theta_0(\eta) + e^{-\varepsilon\tau} H(\eta, \tau), \end{aligned} \quad (30)$$

with  $F(\eta, \tau)$ ,  $G(\eta, \tau)$  and  $H(\eta, \tau)$  (i.e. smaller than  $f_0(\eta)$ ,  $g_0(\eta)$  and  $\theta_0(\eta)$ ) as the disturbances with growth or decay rate of (unknown eigenvalue). The solutions in (30) are then substituted into (26) to (29) to form:

$$\frac{\mu_{hnf}/\mu_f}{\rho_{hnf}/\rho_f} F_0''' + f_0 F_0'' + F_0 f_0'' - 2f_0' F_0' + \varepsilon F_0' = 0, \quad (31)$$

$$\frac{\mu_{hnf}/\mu_f}{\rho_{hnf}/\rho_f} G_0'' - g_0 F_0' - G_0 f_0' + f_0 G_0' + F_0 g_0' + \varepsilon G_0 = 0, \quad (32)$$

$$\frac{1}{Pr} \frac{k_{hnf}/k_f}{(\rho C_p)_{hnf}/(\rho C_p)_f} H_0'' + f_0 H_0' + F_0 \theta_0' + \varepsilon H_0 = 0, \quad (33)$$

$$\begin{aligned} F_0(0) &= 0, \quad F_0'(0) = 0, \quad G_0(0) = 0, \quad H_0(0) = 0 \\ F_0'(\eta) &\rightarrow 0, \quad G_0'(\eta) \rightarrow 0, \quad H_0(\eta) \rightarrow 0 \quad \text{as } \eta \rightarrow \infty \end{aligned} \quad (34)$$

where the initial growth or decay of solutions (30) are given as  $F(\eta) = F_0(\eta)$ ,  $G(\eta) = G_0(\eta)$  and  $H(\eta) = H_0(\eta)$  as  $\tau = 0$ . The above (31) to (34) will yield an infinite set of eigenvalues,  $\varepsilon_1 < \varepsilon_2 < \varepsilon_3 < \dots$  (Awaludin et al. 2016), and the smallest eigenvalue,  $\varepsilon_1$  will determine the stability of the solutions  $f_0(\eta)$ ,  $g_0(\eta)$  and  $\theta_0(\eta)$ . To obtain the possible range of the eigenvalues, one of the boundary conditions is relaxed as follows (Harris et al. 2009):

$$\begin{aligned} F_0(0) &= 0, \quad F_0'(0) = 0, \quad F_0''(0) = 1, \quad G_0(0) = 0, \quad H_0 = 0, \\ G_0'(\eta) &\rightarrow 0, \quad H_0(\eta) \rightarrow 0 \quad \text{as } \eta \rightarrow \infty. \end{aligned} \quad (35)$$

Then, equations (31) to (33) with the new boundary conditions (35) are solved numerically, and the smallest eigenvalue,  $\varepsilon_1$  is computed using the `bvp4c` solver.

#### NUMERICAL SOLUTIONS

The boundary value problem (15) to (18) is solved using a finite-difference code in MATLAB called the `bvp4c` solver. This solver is a residual control based, adaptive mesh solver with the mesh selection and error control based on the residual of the continuous solution (Gökhan 2011; Rosca et al. 2012). This solver uses the `odefun` function which contains the differential equations of the problem, the `bcbfun` function which contains the boundary conditions of the problem, the `solinit` function that receives the initial guess, and the `options` function that holds the integration settings.

The following substitutions are made to rewrite the differential (15) to (17) as first-order differential equations:

$$\begin{aligned} f &= y(1), \quad f' = y(1)' = y(2), \quad f'' = y(2)' = y(3), \quad f''' = y(3)' \\ &= \frac{[-y(1)y(3)-1+(y(2))^2]}{\left[ \frac{\mu_{hnf}/\mu_f}{\rho_{hnf}/\rho_f} \right]} \end{aligned} \quad (36)$$

$$g = y(4), \quad g' = y(4)' = y(5), \quad g'' = y(5)' = \frac{[-y(1)y(5)+y(2)y(4)-\alpha+\beta]}{\left[ \frac{\mu_{hnf}/\mu_f}{\rho_{hnf}/\rho_f} \right]}, \quad (37)$$

$$\theta = y(6), \quad \theta' = y(6)' = y(7), \quad \theta'' = y(7)' = \frac{[-y(1)y(7)]}{\left[ \frac{1}{Pr} \frac{k_{hnf}/k_f}{(\rho C_p)_{hnf}/(\rho C_p)_f} \right]}, \quad (38)$$

and equations (36) to (38) are coded into the `odefun`. Meanwhile, the following boundary conditions are coded into the `bcbfun`:

$$\begin{aligned} ya(1) &= 0, \quad ya(2) = \lambda, \quad ya(4) = 0, \quad ya(6) = 1, \\ yb(2) &\rightarrow 1, \quad yb(5) \rightarrow 1, \quad yb(6) \rightarrow 0 \quad \text{as } \eta \rightarrow \infty. \end{aligned} \quad (39)$$

Initial guesses are then coded into the `solinit` function. Different initial guesses may end up with different solutions that result in several profiles which reach the far-field boundary conditions in (18) asymptotically (Dzulkifli et al. 2018). In this situation, it is said that multiple solutions exist in the boundary value problem. The first solution is decided in such a way that the solution is the first to reach the far-field or free stream conditions.

The validation of the method used in this study is completed by comparing the obtained results with other published results, as shown in Table 3. The results

are found to be in good agreement; thus, verifying the method used. Also, the accuracy of the numerical results is confirmed when the profiles approach the far-field boundary conditions in (18) asymptotically.

$$\begin{aligned}
 F_0 &= y(1), & G_0' &= y(5), & f_0 &= s(1), & g_0' &= s(5), \\
 F_0' &= y(2), & H_0 &= y(6), & f_0' &= s(2), & \theta_0 &= s(6), \\
 F_0'' &= y(3), & H_0' &= y(7), & f_0'' &= s(3), & \theta_0' &= s(7), \\
 G_0 &= y(4), & & & g_0 &= s(4), & &
 \end{aligned}$$

TABLE 3. Comparison of  $f''(0)$  and  $g'(0)$  values when  $\phi_{s1} = \phi_{s2} = 0$ ,  $\lambda = 0$  and  $\alpha = \beta$

Present study		Rahman et al. (2016)		Li et al. (2009)	
$f''(0)$	$g'(0)$	$f''(0)$	$g'(0)$	$f''(0)$	$g'(0)$
1.232588	0.607950	1.23258764	0.60794998	1.23259	0.60777

## RESULTS AND DISCUSSION

The results are displayed in the form of tables and graphs. The effects of various parameters, such as the nanoparticle volume fraction of  $\text{Al}_2\text{O}_3$ ,  $\phi_{s1}$ , the nanoparticle volume fraction of Cu,  $\phi_{s2}$  and the shrinking parameter,  $\lambda$ , on the flow and thermal fields of the fluid are analyzed and discussed.

The identification of a stable solution is made through a stability analysis. Waini et al. (2019) has carried out this analysis to the dual solutions obtained in the flow of aqueous  $\text{Al}_2\text{O}_3$ -Cu hybrid nanofluid. It was discovered that the upper branch solution (i.e. the first solution) is stable, while the lower branch solution (i.e. the second solution) is unstable. Still, to ascertain the stability of solutions obtained in the present problem, the stability analysis is performed, and the results are tabulated in Table 4. From the table, the values of  $\varepsilon_1$  are positive for the first solution but negative for the second solution. Khashi'ie et al. (2019) stated that the negative values of  $\varepsilon_1$  indicate an unstable flow caused by the presence of disturbance, whereas the positive values of  $\varepsilon_1$  imply a stable flow. Hence, it is affirmed that the first solution is stable, while the second solution is unstable in the present problem. The first solution is more significant to this problem and realizable in practice. Nonetheless, the second solution, which is one of the solutions for the boundary problem, is still mathematically meaningful. Therefore, the second solution will be shown but not discussed throughout this section.

Meanwhile, the following substitutions are made to rewrite (31) to (33) and boundary conditions (35) as a system of first-order differential equations for stability analysis:

The plots of  $Re_x C_f$  and  $Re_x^{-1/2} Nu_x$  and for Cu- $\text{Al}_2\text{O}_3$ /H<sub>2</sub>O hybrid nanofluid are presented in Figure 4. Based on these figures, a single solution is obtained at a critical point,  $\lambda_c$ . The solution does not exist when  $\lambda < \lambda_c$  and dual solutions are found when  $\lambda_c < \lambda < -1$ . The increase in  $\phi_{s2}$  reduces the skin friction coefficient of the hybrid nanofluid for the first solution, while the opposite behavior is observed for the second solution. Meanwhile, the value of  $Re_x^{-1/2} Nu_x$  for the first solution is enhanced by the increase in  $\phi_{s2}$ , as shown in Figure 4(b). The thermal conductivity of the hybrid nanofluid is raised by the increase in the nanoparticle volume fraction of Cu (Devi & Devi 2017). However, the local Nusselt number for the second solution is seen to be not affected by the changes in  $\phi_{s2}$ .

The physical quantities of interest (i.e.,  $Re_x C_f$  and  $Re_x^{-1/2} Nu_x$ ) for Cu- $\text{Al}_2\text{O}_3$ /H<sub>2</sub>O hybrid nanofluid and Cu-H<sub>2</sub>O nanofluid are tabulated in Table 5. Based on the table, the values of  $Re_x C_f$  are positive that indicates the hybrid nanofluid exerted a drag force on the sheet. Meanwhile, the positive values of  $Re_x^{-1/2} Nu_x$  imply the transfer of heat from the hot sheet to the hybrid nanofluid. It is noticed that the increase in the magnitude of the shrinking parameter reduces the values of  $Re_x C_f$  and  $Re_x^{-1/2} Nu_x$ . Also, the skin friction coefficient of the hybrid nanofluid is less than the nanofluid, but the local Nusselt number is higher than the nanofluid. On average, the addition of  $\text{Al}_2\text{O}_3$  nanoparticles into the Cu-H<sub>2</sub>O nanofluid reduces the skin friction coefficient by 37.753%, while the

local Nusselt number is enhanced by 4.798%. Therefore, the rate of heat transfer in hybrid nanofluid is higher than in the nanofluid.

Then, the variation of orthogonal flow skin friction,  $f''(0)$ , temperature gradient,  $\theta'(0)$  and oblique flow skin friction,  $g'(0)$  with various values of the shrinking parameter are presented in Tables 6 and 7, respectively. From Tables 6 and 7, the values of  $f''(0)$  and  $g'(0)$  for the first solution decrease when the magnitude of  $\lambda$  increases. However, the opposite trend is observed for the second solution of  $f''(0)$ , while the second solution of  $g'(0)$  remains constant as  $|\lambda|$  increases. Meanwhile, the first solution of  $\theta'(0)$  increases with  $|\lambda|$ . As the free parameter,  $\beta$  can change the shear flow, the effects of this parameter on  $g'(0)$  are analyzed. The values of  $g'(0)$  for both solutions are found to be the highest when  $\beta < \alpha$ . Hence, increasing the value of the free parameter decreases the oblique flow skin friction.

The effects of the shrinking parameter on the dimensionless velocities of the hybrid nanofluid are illustrated in Figure 5(a) and 5(b). In these figures, the increase in  $|\lambda|$  causes the orthogonal velocity,  $f'(\eta)$  and the oblique velocity,  $g'(\eta)$  profiles of the first solution to decrease, in contrast to the second solution. According to Rahman et al. (2016), the shrinking of a sheet will build pressure downstream, which dampens the driving force of the fluid. Consequently, reduces the velocity profiles and velocity gradients, as shown by the first solution in Figure 5(a) and 5(b), and also in Tables 6 and 7.

Next, the effect of  $\lambda$  on the hybrid nanofluid temperature is illustrated in Figure 5(c). From this figure, the increment in the shrinking parameter value raises the temperature profile of Cu-Al<sub>2</sub>O<sub>3</sub>/H<sub>2</sub>O hybrid nanofluid for the first solution, while the opposite occurred for the second solution. The same observation is recorded by Rahman et al. (2016) for nanofluid flow past a shrinking sheet. The positive value of the local Nusselt number when  $\lambda < 0$ , shown in Table 5, indicates that heat is transferred from the hot shrinking sheet to the hybrid nanofluid. The temperature of the hybrid nanofluid is the

highest in the region near the sheet ( $\eta = 0$ ). As the value of  $\eta$  increases, the hybrid nanofluid temperature decreases until it reaches the free stream condition, as obtained in Figure 5(c).

The water-based hybrid Cu-Al<sub>2</sub>O<sub>3</sub> nanofluid is compared with the Cu-H<sub>2</sub>O nanofluid in terms of velocity and temperature. The orthogonal velocity and oblique velocity profiles are shown in Figure 6(a) and 6(b). The figure shows that the velocity profiles of the water-based hybrid Cu-Al<sub>2</sub>O<sub>3</sub> nanofluid and Cu-H<sub>2</sub>O nanofluid increase with the increasing value of  $\phi_{s2}$ . Meanwhile, the nanofluid is seen to have a smaller boundary layer thickness when compared with the hybrid nanofluid. The velocity gradients (i.e.  $f''(0)$  and  $g'(0)$ ) of the nanofluid are higher than the hybrid nanofluid. Therefore, Cu-H<sub>2</sub>O nanofluid has greater skin friction than the water-based hybrid Cu-Al<sub>2</sub>O<sub>3</sub> nanofluid, as obtained in Table 5. Due to the increasing awareness of energy conservation, fluids with low skin friction are preferable in industrial processes. Therefore, the water-based hybrid Cu-Al<sub>2</sub>O<sub>3</sub> nanofluid is more efficient than the Cu-H<sub>2</sub>O nanofluid for industrial purposes.

Next, the temperature profiles of water-based hybrid Cu-Al<sub>2</sub>O<sub>3</sub> nanofluid and Cu-H<sub>2</sub>O nanofluid are presented in Figure 6(c). When  $\lambda < 0$ , the temperature profiles for both solutions diminish as the value of  $\phi_{s2}$  increases. At some distance away from the surface (i.e.,  $\eta > 0$ ), the hybrid nanofluid has a larger thermal boundary layer thickness than the nanofluid. Thus, the temperature gradient,  $\theta'(0)$  of the water-based hybrid Cu-Al<sub>2</sub>O<sub>3</sub> nanofluid is smaller than the temperature gradient of Cu-H<sub>2</sub>O nanofluid.

However, the value of  $Re_x^{-1/2}Nu_x \left( = -\frac{k_{hnf}}{k_f}\theta'(0) \right)$

calculated in Table 5 shows that the heat flux of the hybrid nanofluid is higher than the nanofluid. This result is obtained due to the higher thermal conductivity of the water-based hybrid Cu-Al<sub>2</sub>O<sub>3</sub> nanofluid, compared to the Cu-H<sub>2</sub>O nanofluid (Devi & Devi 2017). Therefore, the water-based hybrid Cu-Al<sub>2</sub>O<sub>3</sub> nanofluid has better heat transfer performance than the Cu-H<sub>2</sub>O nanofluid.

TABLE 4. Smallest eigenvalue, when  $\varepsilon_1$  when  $\phi_{s1} = 0.1$ ,  $\phi_{s2} = 0.005$ ,  $Pr = 6.135$  and  $\alpha = \beta$

$\lambda$	$\varepsilon_1$	
	First solution	Second solution
-1.22	0.432876	-0.398561
-1.23	0.339787	-0.318486
-1.24	0.212052	-0.203639
-1.246	0.062157	-0.061418
-1.2465	0.022977	-0.022875

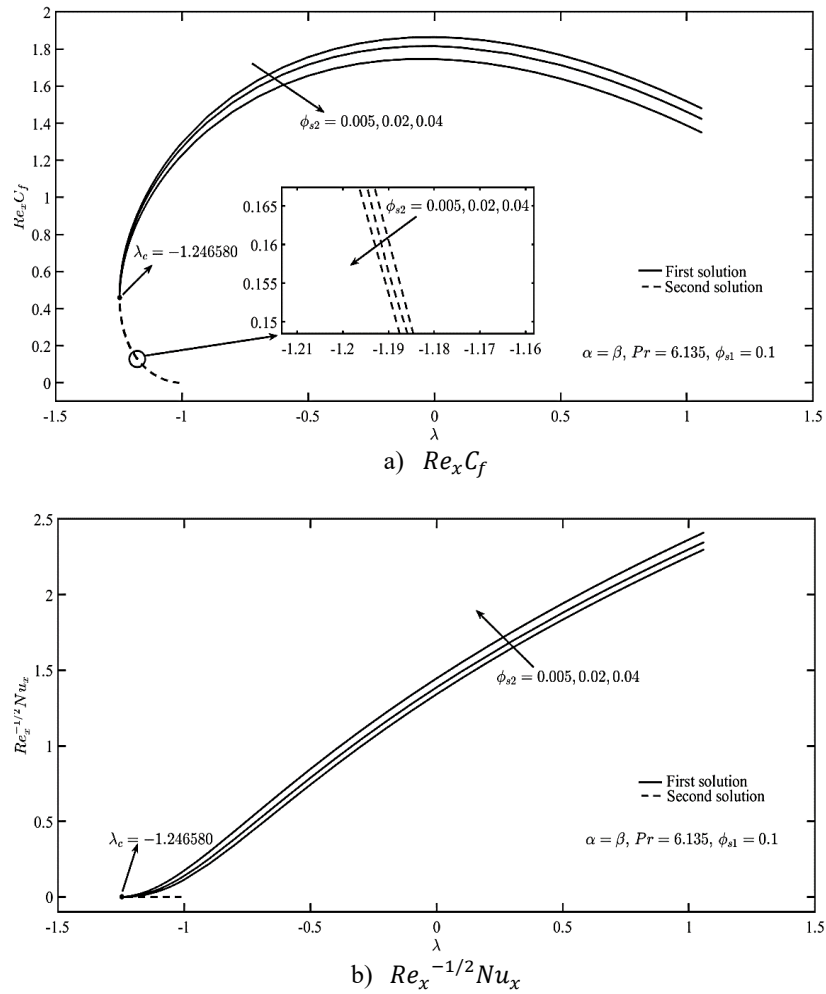


FIGURE 4. Plots of  $Re_x C_f$  and  $Re_x^{-1/2} Nu_x$  for various values of  $\lambda$  and  $\phi_{s2}$

TABLE 5. Values of  $Re_x C_f$  and  $Re_x^{-1/2} Nu_x$  when  $\phi_{s2} = 0.005$ ,  $Pr = 6.135$  and  $\alpha = \beta$

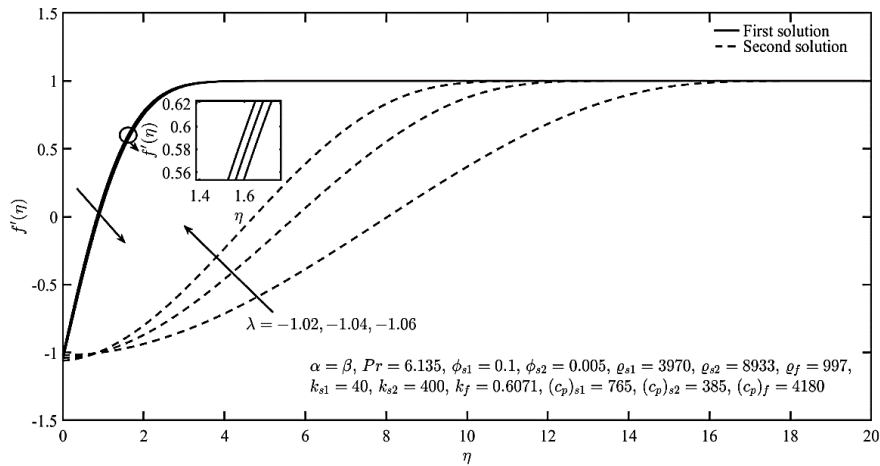
$\lambda$	$\phi_{s1}$	$Re_x C_f$		$Re_x^{-1/2} Nu_x$	
		First solution	Second solution	First solution	Second solution
-1.02	0.1	1.261823	0.001507	0.095546	-0.000000
-1.04		1.227343	0.005971	0.078968	-0.000000
-1.06		1.190686	0.013390	0.063839	-0.000000
-1.02	0.0	1.650129	0.001974	0.040106	0.000000
-1.04		1.605100	0.007819	0.031023	0.000000
-1.06		1.557224	0.017533	0.023284	-0.000000

TABLE 6. Values of  $f''(0)$  and  $\theta(0)$  when  $\phi_{s1} = 0.1$ ,  $\phi_{s2} = 0.005$ ,  $Pr = 6.135$  and  $\alpha = \beta$

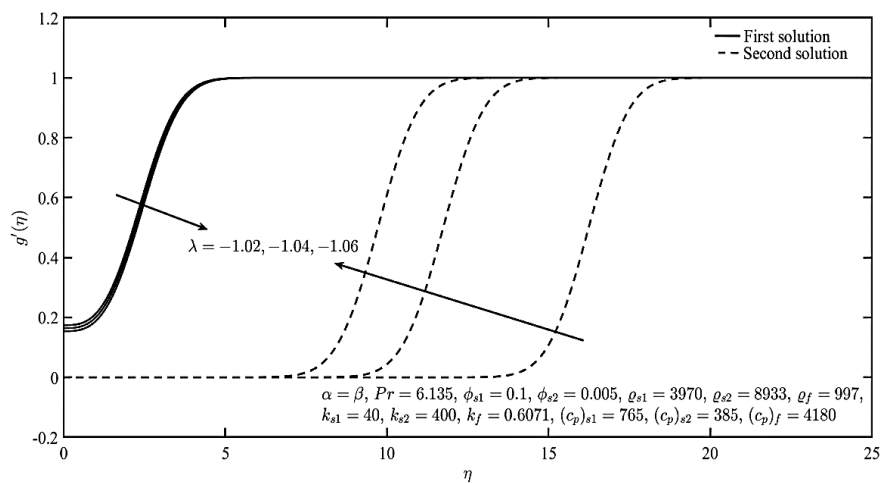
$\lambda$	$f''(0)$		$\theta(0)$	
	First solution	Second solution	First solution	Second solution
-1.02	1.314753	0.001986	-0.071474	-0.000000
-1.04	1.289007	0.007868	-0.059073	-0.000000
-1.06	1.260724	0.017644	-0.047756	-0.000000

TABLE 7. Values of  $g'(0)$  when  $\phi_{s1} = 0.1, \phi_{s2} = 0.005, \alpha = 0.647900$  and  $Pr = 6.135$

$\lambda$	$\beta$	$g'(0)$	
		First solution	Second solution
-1.02	-1	2.392979	34.678952
	1	0.174013	0.000000
-1.04	-1	-0.300105	-7.409710
	1	2.398357	18.039309
-1.06	-1	0.164168	-0.000000
	1	-0.313202	-3.854385
-1.06	-1	2.405391	12.439380
	1	0.154157	0.000000
	1	-0.326856	-2.657871



a)  $f'(\eta)$



b)  $g'(\eta)$

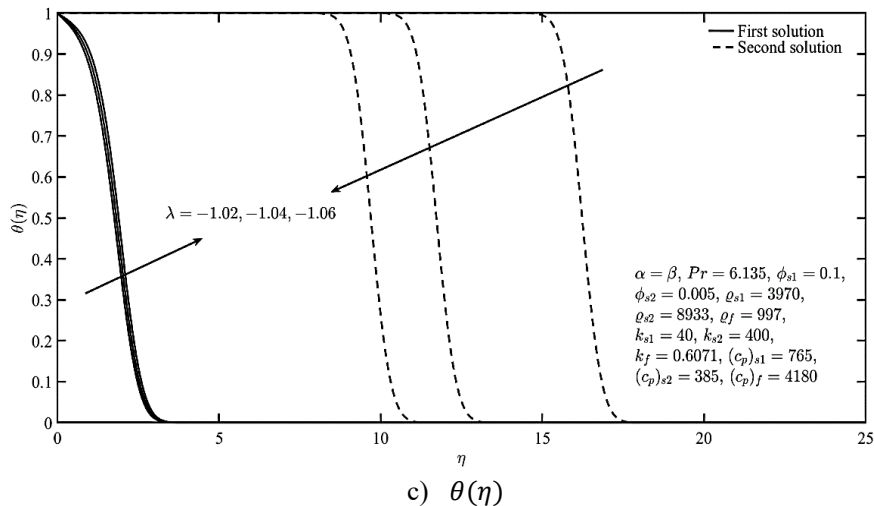
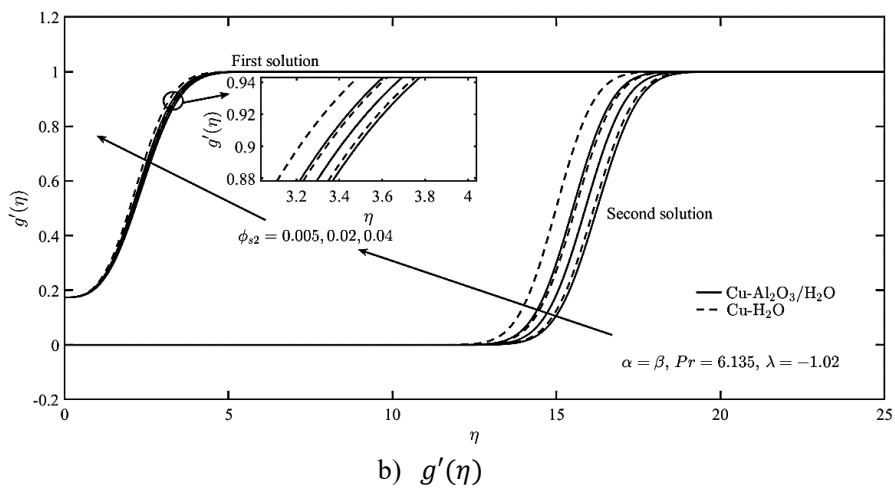
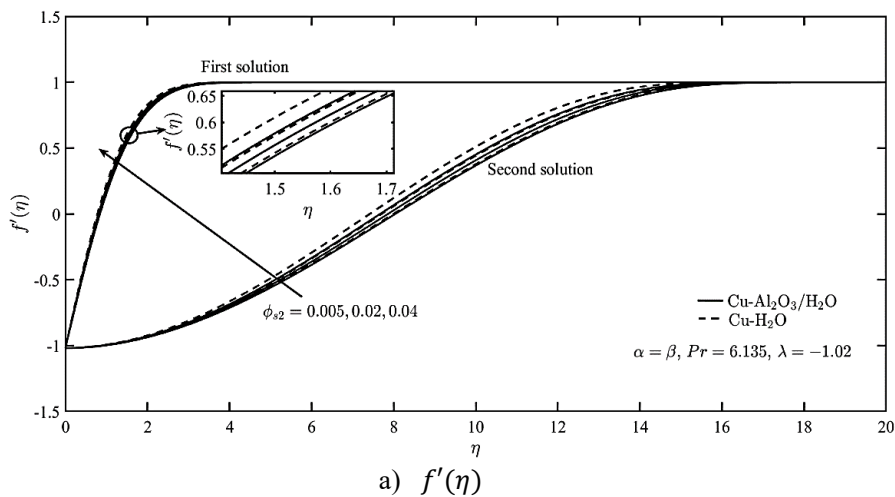


FIGURE 5. Profile plots of dimensionless velocities and temperature for various values of  $\lambda$



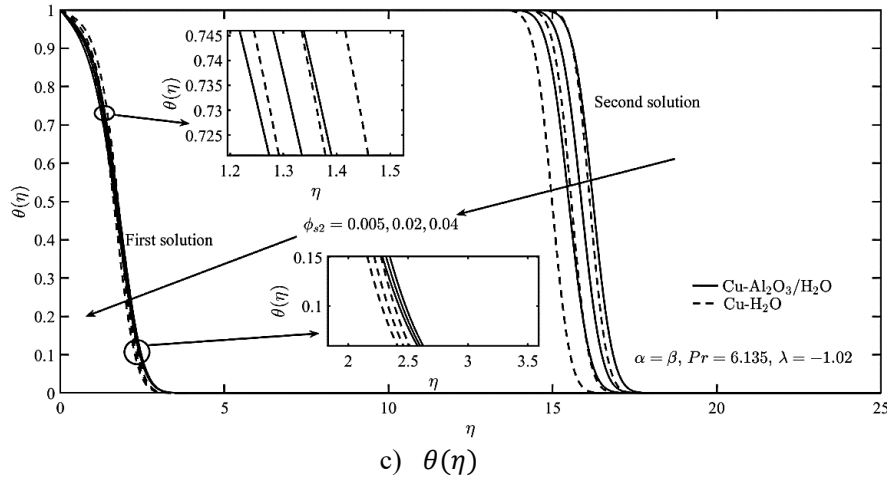


FIGURE 6. Profile plots of dimensionless velocities and temperature for various values of  $\phi_{s2}$

### CONCLUSION

The oblique stagnation-point flow of Cu-Al<sub>2</sub>O<sub>3</sub>/H<sub>2</sub>O hybrid nanofluid over a shrinking surface is studied. The numerical computations result in dual solutions, and the stable solution is decided through a stability analysis. The first solution is found to be stable and thus realizable in real applications, for example, in transpiration cooling. The velocity profiles of Cu-Al<sub>2</sub>O<sub>3</sub>/H<sub>2</sub>O hybrid nanofluid decrease while the temperature profile increases when the shrinking parameter increases. Compared to Cu-H<sub>2</sub>O nanofluid, the Cu-Al<sub>2</sub>O<sub>3</sub>/H<sub>2</sub>O hybrid nanofluid shows improvements in hydrodynamic and heat transfer properties, where the skin friction reduces, and the heat flux increases.

### ACKNOWLEDGEMENTS

The authors gratefully acknowledge the Ministry of Higher Education, Malaysia for the financial support through the Fundamental Research Grant Scheme (KPT FRGS/1/2019/STG06/UPM/02/3, Vot 5540309).

### REFERENCES

- Awaludin, I.S., Weidman, P.D. & Ishak, A. 2016. Stability analysis of stagnation-point flow over a stretching/shrinking sheet. *AIP Advances* 6(4): 045308-1-045308-7.
- Devi, S.P.A. & Devi, S.S.U. 2016. Numerical investigation of hydromagnetic hybrid Cu-Al<sub>2</sub>O<sub>3</sub>/water nanofluid flow over a permeable stretching sheet with suction. *International Journal of Nonlinear Sciences and Numerical Simulation* 17(5): 249-257.

- Devi, S.U. & Devi, S.A. 2017. Heat transfer enhancement of Cu-Al<sub>2</sub>O<sub>3</sub>/water hybrid nanofluid flow over a stretching sheet. *Journal of the Nigerian Mathematical Society* 36(2): 419-433.
- Dorrepal, J.M. 1986. An exact solution of the Navier-Stokes equation which describes non-orthogonal stagnation-point flow in two dimensions. *Journal of Fluid Mechanics* 163: 141-147.
- Drazin, P.G. & Riley, N. 2006. *The Navier-Stokes Equations: A Classification of Flows and Exact Solutions*. Volume 13. Cambridge: Cambridge University Press.
- Dzulkifli, N.F., Bachok, N., Yacob, N.A., Md Arifin, N. & Rosali, H. 2018. Unsteady stagnation-point flow and heat transfer over a permeable exponential stretching/shrinking sheet in nanofluid with slip velocity effect: A stability analysis. *Applied Sciences* 8(11): 2172.
- Ghaffari, A., Javed, T. & Labropulu, F. 2017. Oblique stagnation point flow of a non-newtonian nanofluid over stretching surface with radiation: A numerical study. *Thermal Science* 21(5): 2139-2153.
- Gökhan, F.S. 2011. Effect of the guess function & continuation method on the run time of matlab bvp solvers. *MATLAB-A Ubiquitous Tool for the Practical Engineer*. IntechOpen.
- Grosan, T., Pop, I., Revnic, C. & Ingham, D.B. 2009. Magneto-hydrodynamic oblique stagnation-point flow. *Meccanica* 44(5): 565.
- Harris, S.D., Ingham, D.B. & Pop, I. 2009. Mixed convection boundary-layer flow near the stagnation point on a vertical surface in a porous medium: Brinkman model with slip. *Transport in Porous Media* 77(2): 267-285.
- Hayat, T., Nadeem, S. & Khan, A.U. 2018. Rotating flow of Ag-CuO/H<sub>2</sub>O hybrid nanofluid with radiation and partial slip boundary effects. *The European Physical Journal E* 41(6): 75.

- Hiemenz, K. 1911. Die Grenzschicht an einem in den gleichförmigen Flüssigkeitsstrom eingetauchten geraden Kreiszyylinder. *Dinglers Polytechnisches Journal* 326: 321-324.
- Jamaludin, A., Naganthran, K., Nazar, R. & Pop, I. 2020. MHD mixed convection stagnation-point flow of Cu-Al<sub>2</sub>O<sub>3</sub>/water hybrid nanofluid over a permeable stretching/shrinking surface with heat source/sink. *European Journal of Mechanics-B/Fluids* 84: 71-80.
- Kadhim, H.T., Jabbar, F.A. & Rona, A. 2020. Cu-Al<sub>2</sub>O<sub>3</sub> hybrid nanofluid natural convection in an inclined enclosure with wavy walls partially layered by porous medium. *International Journal of Mechanical Sciences* 186: 105889.
- Kamal, F.A., Zaimi, K., Ishak, A. & Pop, I. 2019. Stability analysis of MHD stagnation-point flow towards a permeable stretching/shrinking sheet in a nanofluid with chemical reactions effect. *Sains Malaysiana* 48(1): 243-250.
- Khashi'ie, N.S., Md Arifin, N., Pop, I., Nazar, R., Hafidzuddin, E.H. & Wahi, N. 2020. Thermal marangoni flow past a permeable stretching/shrinking sheet in a hybrid Cu-Al<sub>2</sub>O<sub>3</sub>/water nanofluid. *Sains Malaysiana* 49(1): 211-222.
- Khashi'ie, N.S., Md Arifin, N., Nazar, R., Hafidzuddin, E.H., Wahi, N. & Pop, I.A. 2019. Stability analysis for magnetohydrodynamics stagnation point flow with zero nanoparticles flux condition and anisotropic slip. *Energies* 12(7): 1268.
- Labropulu, F. & Li, D. 2008. Stagnation-point flow of a second-grade fluid with slip. *International Journal of Non-Linear Mechanics* 43(9): 941-947.
- Li, D., Labropulu, F. & Pop, I. 2009. Oblique stagnation-point flow of a viscoelastic fluid with heat transfer. *International Journal of Non-Linear Mechanics* 44(10): 1024-1030.
- Lok, Y.Y., Mohd Ishak, A. & Pop, I. 2018. Oblique stagnation slip flow of a micropolar fluid towards a stretching/shrinking surface: A stability analysis. *Chinese Journal of Physics* 56(6): 3062-3072.
- Lok, Y.Y., Merkin, J.H. & Pop, I. 2015. MHD oblique stagnation-point flow towards a stretching/shrinking surface. *Meccanica* 50(12): 2949-2961.
- Lok, Y.Y., Pop, I., Ingham, D.B. & Amin, N. 2009. Mixed convection flow of a micropolar fluid near a non-orthogonal stagnation-point on a stretching vertical sheet. *International Journal of Numerical Methods for Heat & Fluid Flow* 19(3/4): 459-483.
- Mahapatra, T.R. & Gupta, A.S. 2002. Heat transfer in stagnation-point flow towards a stretching sheet. *Heat and Mass transfer* 38(6): 517-521.
- Mahmood, K., Sajid, M., Ali, N., Arshad, A. & Rana, M.A. 2017. Effects of lubrication in the oblique stagnation-point flow of a nanofluid. *Microfluidics and Nanofluidics* 21(5): 100.
- Nadeem, S., Ullah, N. & Khan, A.U. 2019. Impact of oblique stagnation point on MHD micropolar nanomaterial in porous medium over an oscillatory surface with partial slip. *Physica Scripta* 94(6): 065209.
- Naganthran, K., Mohd. Nazar, R. & Pop, I. 2017. Stability analysis of impinging oblique stagnation-point flow over a permeable shrinking surface in a viscoelastic fluid. *International Journal of Mechanical Sciences* 131-132: 663-671.
- Rahman, M.M., Grosan, T. & Pop, I. 2016. Oblique stagnation-point flow of a nanofluid past a shrinking sheet. *International Journal of Numerical Methods for Heat & Fluid Flow* 26(1): 189-213.
- Reza, M. & Gupta, A.S. 2010. Some aspects of non-orthogonal stagnation-point flow towards a stretching surface. *Engineering* 2: 705-709.
- Rosca, N.C., Grosan, T. & Pop, I. 2012. Stagnation-point flow and mass transfer with chemical reaction past a permeable stretching/shrinking sheet in a nanofluid. *Sains Malaysiana* 41(10): 1271-1279.
- Sadiq, M.A. 2019. MHD stagnation point flow of nanofluid on a plate with anisotropic slip. *Symmetry* 11: 132.
- Sidik, N.A.C., Adamu, I.M., Jamil, M.M., Kefayati, G.H.R., Mamat, R. & Najafi, G. 2016. Recent progress on hybrid nanofluids in heat transfer applications: A comprehensive review. *International Communications in Heat and Mass Transfer* 78: 68-79.
- Stuart, J.T. 1959. The viscous flow near a stagnation point when the external flow has uniform vorticity. *Journal of the Aerospace Sciences* 26(2): 124-125.
- Suresh, S., Venkataraj, K.P., Selvakumar, P. & Chandrasekar, M. 2012. Effect of Al<sub>2</sub>O<sub>3</sub>-Cu/water hybrid nanofluid in heat transfer. *Experimental Thermal and Fluid Science* 38: 54-60.
- Tamada, K. 1979. Two-dimensional stagnation-point flow impinging obliquely on a plane wall. *Journal of the Physical Society of Japan* 46(1): 310-311.
- Tooke, R.M. & Blyth, M.G. 2008. A note on oblique stagnation-point flow. *Physics of Fluids* 20(3): 033101.
- Turcu, R., Darabont, A., Nan, A., Aldea, N., Macovei, D., Bica, D., Vekas, L., Pana, O., Soran, M., Koos, A. & Biró, L. 2006. New polypyrrole-multiwall carbon nanotubes hybrid materials. *Journal of Optoelectronics and Advanced Materials* 8(2): 643-647.
- Waini, I., Ishak, A. & Pop, I. 2020. Flow and heat transfer of a hybrid nanofluid past a permeable moving surface. *Chinese Journal of Physics* 66: 606-619.
- Waini, I., Mohd Ishak, A. & Pop, I. 2019. Unsteady flow and heat transfer past a stretching/shrinking sheet in a hybrid nanofluid. *International Journal of Heat and Mass Transfer* 136: 288-297.
- Wang, C.Y. 1985. The unsteady oblique stagnation point flow. *The Physics of Fluids* 28(7): 2046-2049.
- Weidman, P.D., Kubitschek, D.G. & Davis, A.M.J. 2006. The effect of transpiration on self-similar boundary layer flow over moving surfaces. *International Journal of Engineering Science* 44: 730-737.

Rusya Iryanti Yahaya & Norihan Md Arifin\*  
 Institute for Mathematical Research  
 Universiti Putra Malaysia  
 43400 UPM Serdang, Selangor Darul Ehsan  
 Malaysia

Norihan Md Arifin\*  
Department of Mathematics  
Universiti Putra Malaysia  
43400 UPM Serdang, Selangor Darul Ehsan  
Malaysia

Roslinda Mohd. Nazar  
School of Mathematical Sciences  
Faculty of Science and Technology  
Universiti Kebangsaan Malaysia  
43600 UKM Bangi, Selangor Darul Ehsan  
Malaysia

Ioan Pop  
Department of Mathematics  
Babeş-Bolyai University  
400084 Cluj-Napoca  
Romania

\*Corresponding author; email: [norihanarifin@yahoo.com](mailto:norihanarifin@yahoo.com)

Received: 12 October 2020

Accepted: 2 February 2021